PHYSICAL REVIEW B **91**, 201409(R) (2015)

Spectroscopic evidence in the visible-ultraviolet energy range of surface functionalization sites in the multilayer Ti_3C_2 MXene

Damien Magne,[1] Vincent Mauchamp,[1,*] Stéphane Célérier,[2] Patrick Chartier,[1] and Thierry Cabioc'h[1]

[1]*Institut Pprime, UPR 3346 CNRS–Université de Poitiers–ISAE-ENSMA, Boîte Postale 30179, 86962 Futuroscope-Chasseneuil Cedex, France*

[2]*Institut de Chimie des Milieux et Matériaux de Poitiers (IC2MP), UMR CNRS 7285, Faculté des Sciences Fondamentales et Appliquées, Université de Poitiers, 4, rue Michel Brunet, Bâtiment B27, TSA 51106, 86073 Poitiers Cedex 9, France*

(Received 17 February 2015; revised manuscript received 22 April 2015; published 21 May 2015)

Valence electron energy-loss (VEEL) spectroscopy in the transmission electron microscope is combined to *ab initio* calculations to investigate the dielectric properties of multilayer (ML) two-dimensional $Ti_3C_2T_2$ ($T \equiv$ OH or F) MXene. Besides evidencing important similarities between the ML-$Ti_3C_2T_2$ and TiC valence electron gas behaviors, a clear interband transition characteristic of the most stable site of the T functionalization groups is identified in the VEEL spectrum. This signature, highly dependent on the T-group localization on the surface, has a prominent effect on the optical properties of the ML, leading to 40% variations in the optical conductivity in the middle of the visible spectrum. Such a dependence could be of crucial interest for optical transparent thin films or sensing applications.

DOI: 10.1103/PhysRevB.91.201409 PACS number(s): 78.67.−n, 79.20.Uv, 78.20.Bh, 71.20.Be

Since the discovery of graphene and its supreme properties [1], there is a tremendous interest in two-dimensional (2D) systems, the physics governing their properties being significantly different from bulk materials. In this dynamic context, a new group of 2D transition metal carbides or carbonitrides, described as "2D-conductive clays" [2], was recently discovered [3]. These compounds, called MXenes, are produced by etching the Al layers from nanolaminated ternary carbides or nitrides called $M_{n+1}AX_n$ phases (M being a transition metal, A being Al, and X is either C or N) [4]. The chemical process leading to the synthesis of MXenes results in weakly interacting 2D metallic MX sheets passivated by OH and/or F surface termination groups T [see Figs. 1(a) and 1(b)] [5,6]. Depending on the value of n in the parent $M_{n+1}AX_n$ compound, these MX sheets are three, five or seven (M,X) atomic layers thick and given the versatility of the MAX phase compositions, the MXene family is expected to be particularly large.

Among the many MXenes reported to date, $Ti_3C_2T_2$ is by far the most studied: it has been shown to exhibit outstanding intercalation properties with very promising applications for supercapacitors or lithium or non-lithium ion batteries [(N)LIB] [7–9], peculiar optical properties combining optical transparency and enhanced surface plasmons [10,11], among others. The T surface groups localization on top of the MXene sheet and/or their chemical nature, play a key role in these properties: they affect the capacity for energy storage applications [9,12], influence the surface plasmon resonance [11], or eventually induce magnetism and open a band gap [13]. The T groups have thus attracted much attention especially from a theoretical point of view [14,15]. Density functional theory (DFT) calculations, essentially performed on MXene single sheets, predict two stable sites for T: the so-called configuration 1 (C1) where the T groups are above the hollow sites of three neighboring X atoms, and configuration 2 (C2) where the T groups are located above the X atoms. A third configuration (C3) can be considered, with configurations 1 and 2 on each side of the MXene slab [see Figs. 1(a) and 1(b) for a sketch of configuration C3]. To the best of our knowledge, the only experimental attempt to give insights into these termination groups was performed by Shi *et al.* using atomic pair distribution function (PDF) [16]. Beyond the structural parameters obtained from PDF, it is very important to obtain experimental signatures of these terminations at the single object level and investigate their effect in terms of electronic structure: this is particularly important as far as energy storage, electrical and optical properties, as well as potential sensing applications are concerned.

In the present study, we evidence the role of the T groups on the electronic structure and related optical properties of multilayer (ML) $Ti_3C_2T_2$ using the combination of valence electron energy-loss spectroscopy (VEELS) performed in a transmission electron microscope (TEM) [17] and *ab initio* calculations. The choice for VEELS is motivated by the versatile information that can be retrieved at the nanometer scale. Because it is related to the dielectric response of the system through the loss function $\mathrm{Im}[-1/\varepsilon(\mathbf{q},\omega)]$, VEELS combines information on the global valence electron gas, including nanostructuration effects [18–20], related physical properties [21,22], and detailed information on the band structure [23,24]. In addition, since the VEELS signal is much more intense than the corresponding core-loss excitations, the acquisition times are significantly reduced thereby minimizing the irradiation damage in the sample [25]: this is particularly important for the study of the T groups.

The $Ti_3C_2T_2$ samples were prepared as described in the literature by etching the Al from Ti_3AlC_2 powder using hydrofluoric acid [3,6]. The TEM samples were then prepared by blowing the $Ti_3C_2T_2$ powders into air before picking them up on a Cu grid covered with lacy carbon films. The ML-MXenes sheets, which are several hundreds of nanometers long, were probed with the electron beam perpendicular to the sheets. The VEELS spectra were recorded in image mode in a JEOL 2200FS microscope equipped with an in-column omega filter and operated at 200 kV. The energy resolution

*vincent.mauchamp@univ-poitiers.fr

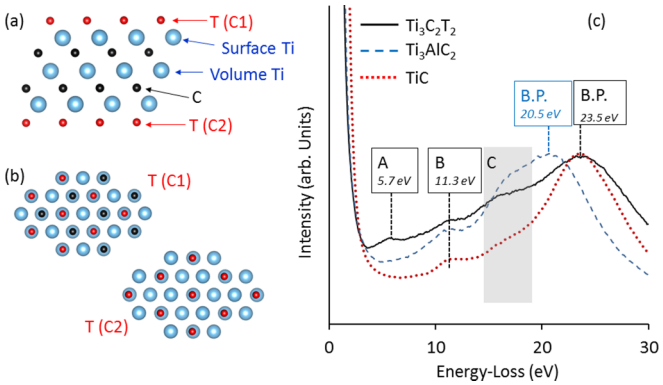

FIG. 1. (Color online) (a) Side view of a $Ti_3C_2T_2$ single sheet evidencing the C3 configuration with the T groups in C1 and C2 on each side of the sheet. (b) Top views corresponding to the C1 and C2 configurations. (c) Experimental VEEL spectra recorded on ML-$Ti_3C_2T_2$ (full black lines), $Ti_3Al_2C_2$ (dashed blue lines), and TiC (red dotted lines).

determined from the zero-loss peak full width at half maximum was 0.8 eV. Spectra recorded on ML-$Ti_3C_2T_2$ with typical thickness of 0.3 times the inelastic mean free path were selected. In order to minimize irradiation damage, parallel illumination was used and acquisition times were 0.1 s per spectrum. In these conditions, the estimated electron dose per acquisition is around 50 electrons/Å^2 and the probed area, defined by the spectrometer aperture, is a disk of approximately 30 nm radius. The collection angle was 7 mRad: in these conditions we mainly probe the basal plane response of the sample (i.e., the momentum transfer $\mathbf{q}$ is mainly parallel to the MXene sheets). Using these experimental conditions, we neither observe changes in the spectra nor modifications in the corresponding image contrast as reported in sensitive samples [26,27].

A typical ML-$Ti_3C_2T_2$ experimental VEEL spectrum is sketched in Fig. 1(c): four distinct structures, labeled A–C and B.P. (for bulk plasmon), are evidenced. This spectrum is compared to those recorded in the same conditions on the corresponding Ti_3AlC_2 MAX phase and a TiC reference sample. Figure 1(c) reveals striking similarities between the ML-$Ti_3C_2T_2$ and TiC valence electron gases: structures B, C and the B.P. lie at the same energy position, in contrast with Ti_3AlC_2 for which the B.P. is 3 eV below. Such similarities in the behavior of the valence electron gas in ML-$Ti_3C_2T_2$ and TiC could result in similar properties. As an example, following the empirical correlation established between the B.P. energy and mechanical properties (e.g., Young modulus, bulk modulus, shear modulus, etc.) in many materials [21], our results give support to the DFT calculations which predict some of the MXene mechanical properties to be very similar to those of TiC and different from Ti_3AlC_2 [3].

Figure 1(c) reveals a noticeable difference between the three compounds. The structure A at 5.7 eV, which is clearly evidenced in the VEEL spectrum of ML-$Ti_3C_2T_2$, is absent from the other spectra: it is thus characteristic of the MXene electronic structure. In order to get deeper insights into the origin of structure A, the MXene basal plane dielectric response in the optical limit, i.e., $\varepsilon_{xx}(\mathbf{0},\omega) = \varepsilon_{1,xx}(\mathbf{0},\omega) + i\,\varepsilon_{2,xx}(\mathbf{0},\omega)$, and related VEEL spectrum are investigated using DFT calculations performed on different structural models [28]. In our models, the ML-$Ti_3C_2T_2$ is described as a periodic stack of two MXene sheets, in agreement with the unit-cell parameters determined from Rietveld refinements of powder x-ray diffractograms ($a = b = 3.058$ Å, $c = 19.599$ Å, $\alpha = 93.234°$, $\beta = 87.459°$, and $\gamma = 120.161°$). Different configurations were considered for the surface groups: either in C1, C2, or in all possible C3 for each one of the two MXene sheets of the unit cell. The atomic positions were then optimized, keeping the experimental unit-cell parameters constant, using the Vienna *Ab Initio* Simulation Package with projector augmented wave (PAW) potentials [29,30]. Calculations were performed in the generalized gradient approximation as parametrized by Perdew *et al.* (GGA-PBE) [31]. This choice is justified by the fact that GGA-PBE has been shown to provide accurate atomic positions in molecular crystals for fixed unit-cell parameters [32]. A 900 eV cutoff was used and the PAW atomic configurations were $2s^2\,2p^2$ for C, $2s^2\,2p^5$ for F, $2s^2\,2p^4$ for O, and $3p^6\,3d^2\,4s^2$ for Ti. Calculations were performed using a $22 \times 22 \times 2$ k-point grid and forces were converged to better than 0.01 eV/Å.

As reported for $Ti_3C_2T_2$ single sheets [15], configuration C1 is found to be more stable than C2, the energy difference being 0.979 eV for $T \equiv$ OH and 1.674 eV for $T \equiv F$ [see Fig. 2(a)]. The various C3 configurations are in between these two situations: all configurations differ from C1 by more than 0.3 eV with the noticeable exception of a OH-terminated configuration, labeled $C3_1$ and also presented in Fig. 2(a). In this configuration, the central MXene sheet is in the configuration C3 depicted in Fig. 1(a). This last configuration differs from C1 by only 0.081 eV. Such a small difference evidences the influence of the stacking on the position of the T groups in ML-MXenes. In this particular case, the intercalation of a C2 surface [marked by an arrow in the $C3_1$ configuration of Fig. 2(a)] between C1 configurations reduces the interaction between adjacent OH terminations. Considering these results, structures C1 and C2 for $Ti_3C_2F_2$ and C1, C2, and $C3_1$ for $Ti_3C_2(OH)_2$ were used as inputs for the computation of the VEEL spectra.

The VEEL spectra corresponding to each structural model were computed from the basal plane dielectric function $\varepsilon_{xx}(\mathbf{0},\omega)$. Since electron-hole interactions were shown to be negligible in the basal plane response of MAX phases and MXenes alike [11,23], calculations were performed in the independent particle approximation, using the OPTIC package of WIEN2K [33]. In this approach, the energy dependent imaginary part of the dielectric function is computed as the sum of the p_x momentum operator matrix elements taken between valence and conduction Kohn-Sham orbitals [$\Psi_k^{v,c}$ with energies $\epsilon_{c,v}(\mathbf{k})$] obtained in the augmented plane wave+local orbitals method [34]:

$$\varepsilon_{2,xx}(\mathbf{0},\omega) \propto \frac{1}{\omega^2} \sum_{v,c} \int d\mathbf{k} \langle \Psi_k^c | \mathbf{p}_x | \Psi_k^v \rangle \langle \Psi_k^v | \mathbf{p}_x | \Psi_k^c \rangle \times \delta(\epsilon_c(\mathbf{k}) - \epsilon_v(\mathbf{k}) - \omega). \quad (1)$$

The real part of $\varepsilon_{xx}(\mathbf{0},\omega)$ is then deduced from a Kramers-Kronig transformation. Exchange and correlation effects were treated using the GGA-PBE. The plane wave expansion was

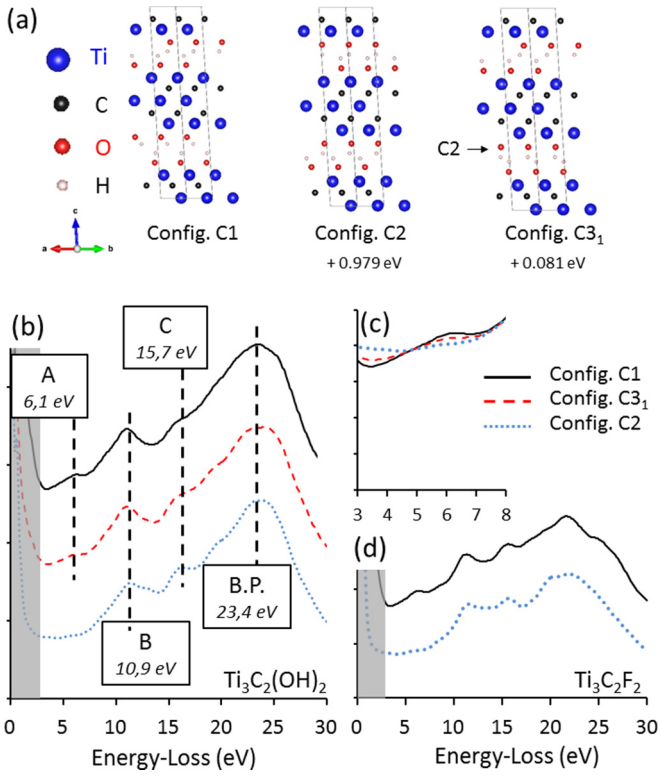

FIG. 2. (Color online) (a) Schematic of the three configurations considered for the calculations of the $Ti_3C_2(OH)_2$ VEEL spectra. Numbers for C2 and $C3_1$ give the energy difference with respect to the most stable configuration: C1. For $C3_1$, the OH layer in C2 is evidenced by an arrow. (b) Theoretical VEEL spectra of the different $Ti_3C_2(OH)_2$ configurations. (c) Enlargement of the energy range corresponding to structure A in (b). (d) Theoretical VEEL spectra of the C1 and C2 configurations of $Ti_3C_2F_2$. The gray shaded areas are disregarded since they are hidden by the zero-loss peak in our experiments.

converged for a $RK_{\max} = 3.5$, with muffin-tin radii of 1.72, 2.10, 1.18, and 0.64 for Ti, C, O, and H, respectively for $T \equiv$ OH, and $RK_{\max} = 7.5$, with muffin-tin radii of 1.74, 2.07, and 1.97 for Ti, C and F for $T \equiv$ F. The dielectric functions were computed using 2500 k points and a Lorentzian broadening of 0.8 eV, corresponding to the experimental energy resolution, was applied. The electron inelastic cross section (i.e., the VEEL spectrum) was then obtained by integrating, on the collection angle, the Kröger cross section for thin films taking $\varepsilon_{xx}(\mathbf{0},\omega)$ and the sample thickness as inputs [35]. The corresponding theoretical VEEL spectra are given in Fig. 2(b) for $T \equiv$ OH and (d) $T \equiv$ F. The energy range corresponding to the structure A is enlarged in Fig. 2(c) for $T \equiv$ OH.

The theoretical VEEL spectra corresponding to models C1 or $C3_1$ [see Fig. 2(b)] nicely reproduce the experimental spectrum of Fig. 1(c): structures A–C and the B.P. are found with at most a 0.5 eV error with respect to the experimental energy positions. Comparing the calculated spectra of C1 and $C3_1$ with that of C2, one hardly sees any difference except for structure A, which is absent from C2. This particular structure is thus characteristic of the T surface group. This is clearly evidenced in Fig. 2(c): the spectrum of C2 is flat in the energy

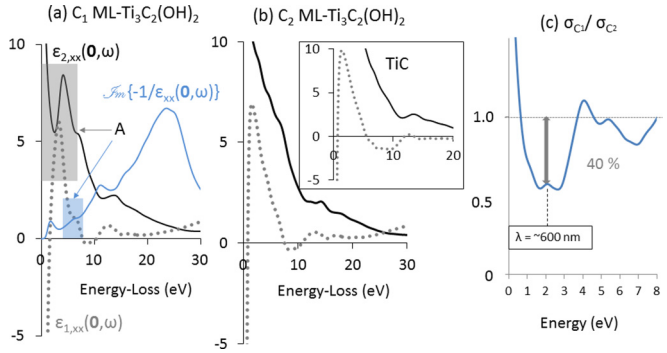

FIG. 3. (Color online) Imaginary (full black line) and real (gray dots) parts of $\varepsilon_{xx}(\mathbf{0},\omega)$ for (a) C1 ML-$Ti_3C_2(OH)_2$ and (b) C2 ML-$Ti_3C_2(OH)_2$ (inset: same quantities for TiC). In (a) the bulk loss function is also shown. (c) Ratio of the basal plane optical conductivity $\sigma_{xx}(\mathbf{0},\omega) = \frac{\omega}{4\pi}\varepsilon_{2,xx}(\mathbf{0},\omega)$ between the C1 and C2 configurations.

range of structure A, whereas the structure is clearly marked for C1 and $C3_1$. That the feature A is observable in $C3_1$ is not surprising since this model is close to C1. It is interesting to observe that structure A is determined by the position of the surface group (C1 or C2) rather than its chemical nature. This is clearly evidenced in the case of $Ti_3C_2F_2$ where the structure A is also observed for C1 and vanishes for C2 [see Fig. 2(d)]: this structure is thus a signature of the MXene functionalization site. Our calculations also show that, although it has little influence on structure A, the chemical nature of T has a strong influence on the relative intensities of structures B and C as well as on the B.P. shape. Given that the agreement with experiment is clearly not as good for $T \equiv$ F as compared to T ≡ OH, we conclude that our ML-$Ti_3C_2T_2$ is predominantly terminated with OH groups.

The origin of structure A can be rationalized in terms of interband transitions (IBT) between Kohn-Sham orbitals by investigating the dielectric response of the system: $\varepsilon_{1,xx}(\mathbf{0},\omega)$ and $\varepsilon_{2,xx}(\mathbf{0},\omega)$ for the C1 ML-$Ti_3C_2(OH)_2$ are given in Fig. 3(a) and compared to those of C2 ML-$Ti_3C_2(OH)_2$ and TiC in Fig. 3(b). Structure A clearly originates from an intense IBT centered around 4 eV (gray area) in $\varepsilon_{2,xx}(\mathbf{0},\omega)$. That this peak arises at lower energy compared to its equivalent in the loss function is due to the screening effect resulting from the denominator of the loss function [i.e., $\varepsilon^*_{xx}(\mathbf{0},\omega).\varepsilon_{xx}(\mathbf{0},\omega)$] [36]. This peak, clearly marked out of the decreasing background in C1 ML-$Ti_3C_2(OH)_2$, is lost for C2 leading to a dielectric response very similar to that of TiC in the corresponding energy range [see inset of Fig. 3(b)]. Since this IBT has a prominent effect on $\varepsilon_{2,xx}(\mathbf{0},\omega)$, it affects the ML-MXene optical properties. In particular, as evidenced in Fig. 3(c), the change in the surface group location leads to a 40% drop in the optical conductivity when going from a C2 to a C1 configuration. This drop occurs in the middle of the visible spectrum, which is particularly interesting for transparent conductive films or sensing applications [10].

The observed changes in the dielectric response of the system as a function of the functionalization site is directly related to its electronic structure. The electron density of states (DOS) decomposed on O, C, volume and surface Ti are given in Fig. 4 for C1 (top) and C2 ML-$Ti_3C_2(OH)_2$ (bottom).

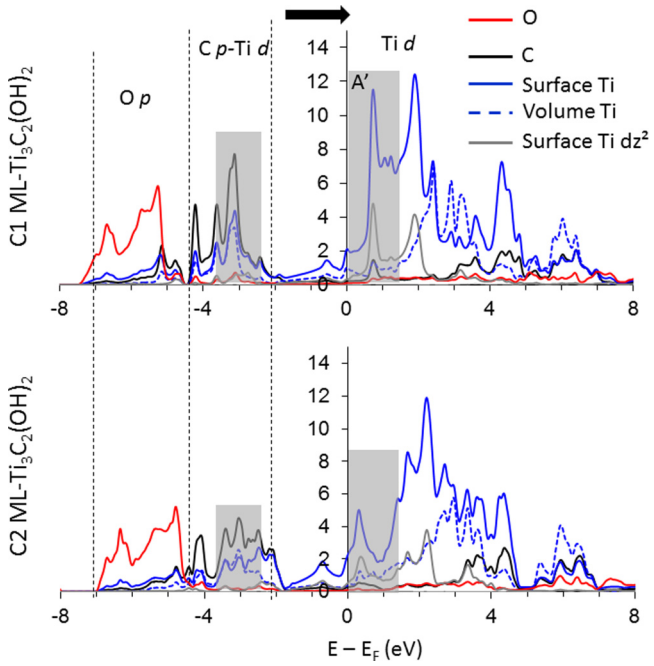

FIG. 4. (Color online) Site projected DOS of C1 ML-$Ti_3C_2(OH)_2$ (top) and C2 ML-$Ti_3C_2(OH)_2$ (bottom). The energy range corresponding to the initial and final states involved in peak A are marked by gray areas. The contribution from hydrogen atoms is disregarded since it is negligible.

Basically, these DOS exhibit very similar general trends: the valence band is built on low-lying O p states (between -7.5 and -4.5 eV), hybridizations between C p and Ti d states (between -4.5 and -2 eV) and dominated by Ti d states from -2 eV up to 8 eV above E_F with increasing hybridizations with O and C above 3 eV. From the decomposition of Eq. (1) among all possible transitions between valence and conduction bands, peak A is evidenced as being due to transitions from seven occupied bands centered around 3 eV below E_F up to nine empty bands centered around 0.8 eV above E_F [28]: the energy range corresponding to these states is marked by gray areas in Fig. 4. The main difference obviously comes from the empty states: a prominent peak (peak A') is observed in the corresponding energy range for C_1, whereas it is absent for C_2. As evidenced by the gray line, this peak arises from the hybridization between the surface Ti dz^2 and C p orbitals: the modification of the MXene optical properties with the T group site thus results from an orbital reconstruction in the TiC layers. This could be related to the fact that the C-O distance in the C2 configuration is 25% smaller than for the C1 one, others distances (Ti-C, Ti-O) being similar [see Figs. 1(a) and 1(b)]. Given the electronegativity of the oxygen, such a decrease in the C-O length could compete with the Ti-C bond and reduce the Ti-C hybridization leading to the vanishing of the corresponding peak in the DOS.

In conclusion, the dielectric properties and related VEEL spectra of ML-$Ti_3C_2T_2$ have been investigated in the visible-UV range. Besides evidencing important similarities between the MXene and TiC valence electron gases, a clear spectroscopic signature of the MXene most stable surface functionalization sites is evidenced in the VEEL spectrum. Such a structure offers the possibility to investigate the surface functionalization in ML-$Ti_3C_2T_2$ at the nanometer scale. On the basis of DFT calculations, this signature is identified as an interband transition involving the surface Ti dz^2 orbitals hybridized with C p states. These states, very sensitive to the T groups localization on the MXene surface, largely influence the optical properties of the MXene. They induce a 40% variation of the optical conductivity in the middle of the visible spectrum and are thus expected to play a crucial role for optical or sensing applications among others.

We are grateful to the computational facilities of the Pprime Institute. This work has been supported by the "Région Poitou-Charentes."

[1] K. S. Novoselov, V. I. Fal'ko, L. Colombo, P. R. Gellert, M. G. Schwab, and K. Kim, Nature (London) **490**, 192 (2012).
[2] M. Ghidiu, M. R. Lukatskaya, M. Q. Zhao, Y. Gogotsi, and M. W. Barsoum, Nature (London) **516**, 78 (2014).
[3] M. Naguib, V. N. Mochalin, M. W. Barsoum, and Y. Gogotsi, Adv. Mater. **26**, 992 (2014).
[4] M. W. Barsoum, *MAX Phases: Properties of Machinable Ternary Carbides and Nitrides* (Wiley, New York, 2013).
[5] M. Naguib, M. Kurtoglu, V. Presser, J. Lu, J. Niu, M. Heon, L. Hultman, Y. Gogotsi, and M. W. Barsoum, Adv. Mater. **23**, 4248 (2011).
[6] M. Naguib, O. Mashtalir, J. Carle, V. Presser, J. Lu, L. Hultman, Y. Gogotsi, and M. W. Barsoum, ACS Nano **6**, 1322 (2012).
[7] M. R. Lukatskaya, O. Mashtalir, C. E. Ren, Y. Dall'Agnese, P. Rozier, P. L. Taberna, M. Naguib, P. Simon, M. W. Barsoum, and Y. Gogotsi, Science **341**, 1502 (2013).
[8] O. Mashtalir, M. Naguib, V. N. Mochalin, Y. Dall'Agnese, M. Heon, M. W. Barsoum, and Y. Gogotsi, Nat. Commun. **4**, 1716 (2013).
[9] Y. Xie, Y. Dall'Agnese, M. Naguib, Y. Gogotsi, M. W. Barsoum, H. L. Zhuang, and Paul R. C. Kent, ACS Nano **8**, 9606 (2014).
[10] J. Halim, M. R. Lukatskaya, K. M. Cook, J. Lu, C. Smith, L. Å Näslund, S. J. May, L. Hultman, Y. Gogotsi, P. Eklund, and M. W. Barsoum, Chem. Mater. **26**, 2374 (2014).
[11] V. Mauchamp, M. Bugnet, E. P. Bellido, G. A. Botton, P. Moreau, D. Magne, M. Naguib, T. Cabioc'h, and M. W. Barsoum, Phys. Rev. B **89**, 235428 (2014).
[12] Y. Xie, M. Naguib, V. N. Mochalin, M. W. Barsoum, Y. Gogotsi, X. Yu, K.-W. Nam, X.-Q. Yang, A. I. Kolesnikov, and P. R. C. Kent, J. Am. Chem. Soc. **136**, 6385 (2014).
[13] M. Khazaei, M. Arai, T. Sasaki, C.-Y. Chung, N. S. Venkataramanan, M. Estili, Y. Sakka, and Y. Kawazoe, Adv. Funct. Mater. **23**, 2185 (2013).
[14] A. N. Enyashin and A. L. Ivanovskii, Comput. Theor. Chem. **989**, 27 (2012).
[15] Y. Xie and P. R. C. Kent, Phys. Rev. B **87**, 235441 (2013).
[16] C. Shi, M. Beidaghi, M. Naguib, O. Mashtalir, Y. Gogotsi, and S. J. L. Billinge, Phys. Rev. Lett. **112**, 125501 (2014).

[17] R. F. Egerton, *Electron Energy-Loss Spectroscopy in the Electron Microscope* (Plenum, New York, 1995).
[18] F. S. Hage, Q. M. Ramasse, D. M. Kepaptsoglou, Ø. Prytz, A. E. Gunnaes, G. Helgesen, and R. Brydson, Phys. Rev. B **88**, 155408 (2013).
[19] N. Jiang, D. Su, J. C. H. Spence, and A. Howie, Appl. Phys. Lett. **94**, 253105 (2009).
[20] Z. Xu, Y. Bando, L. Liu, W. Wang, X. Bai, and D. Golberg, ACS Nano **5**, 4401 (2011).
[21] V. P. Oleshko, M. Murayama, and J. M. Howe, Microsc. Microanal. **8**, 350 (2002).
[22] F. A. Gutierrez, J. Díaz-Valdés, and H. Jouin, J. Phys.: Condens. Matter. **19**, 326221 (2007).
[23] V. Mauchamp, G. Hug, M. Bugnet, T. Cabioc'h, and M. Jaouen, Phys. Rev. B **81**, 035109 (2010).
[24] M. Launay, F. Boucher, and P. Moreau, Phys. Rev. B **69**, 035101 (2004).
[25] M. Koshino, H. Kurata, and S. Isoda, Ultramicroscopy **110**, 1465 (2010).
[26] R. F. Egerton, S. Lazar, and M. Libera, Micron **43**, 2 (2012).
[27] N. Jiang and J. C. H. Spence, Ultramicroscopy **111**, 860 (2011).
[28] See Supplemental Material at http://link.aps.org/supplemental/10.1103/PhysRevB.91.201409 for (i) a discussion concerning the anisotropy of the ML-$Ti_3C_2T_2$ dielectric tensor and (ii) the decomposition of $\varepsilon_{xx}(0,\omega)$ among the different valence to conduction band transitions for the C1 ML-$Ti_3C_2(OH)_2$.
[29] G. Kresse and J. Furthmüller, Phys. Rev. B **54**, 11169 (1996).
[30] G. Kresse and D. Joubert, Phys. Rev. B **59**, 1758 (1999).
[31] J. P. Perdew, K. Burke, and M. Ernzerhof, Phys. Rev. Lett. **77**, 3865 (1996).
[32] J. Binns, M.-R. Healy, S. Parsons, and C. A. Morrison, Acta Crystallogr., Sect. B: Struct. Sci., Cryst. Eng. Mater. **70**, 259 (2014).
[33] C. Ambrosch-Draxl and J. O. Sofo, Comput. Phys. Commun. **175**, 1 (2006).
[34] P. Blaha, K. Schwarz, G. K. H. Madsen, D. Kvasnicka, and J. Luitz, *WIEN2K, an Augmented Plane Wave+Local Orbitals Program for Calculating Crystal Properties* (Karlheinz Schwarz, Techn. Universität Wien, Austria, 2001).
[35] E. Kröger, Z. Phys. **235**, 403 (1970).
[36] A. Alkauskas, S. D. Schneider, C. Hébert, S. Sagmeister, and C. Draxl, Phys. Rev. B **88**, 195124 (2013).